

Review

Recent Progress in Synthesis and Photonic Applications of Two-Dimensional Bismuthene

Haoran Li and Zhibin Yang * 

Center for Terahertz Waves and College of Precision Instrument and Optoelectronics Engineering,
Tianjin University, Tianjin 300072, China

* Correspondence: zbyang0417@tju.edu.cn

Abstract: The emergence of phosphorene has generated significant interest in 2D group VA nano-materials. Among this group, bismuthene exhibits layer-dependent direct bandgaps, high carrier mobility, and topological insulator properties because of its unique structure and ultrathin nature, distinguishing it as a promising candidate for photonic applications. Particularly, its outstanding stability in air makes bismuthene more advantageous than phosphorene for practical applications. Here, we provide a comprehensive review of recent advances regarding 2D bismuth by focusing on the aspects of methods of synthesis and photonic applications. First, the structure and fundamental properties of bismuthene are described, referring to its crystallinity and band structures, as well as to its nonlinear optical properties. Subsequently, the common synthesis methods for 2D bismuth are summarized, including both top-down and bottom-up approaches. Then, potential photonic applications based on 2D bismuth, involving nonlinear photonic devices, photocatalyst, and photodetectors, are illustrated. The performance, mechanisms, and features of the devices are discussed. Finally, the review is summarized and some challenges and future outlooks in this field are addressed.

Keywords: photonics; 2D materials; bismuthene; photodetectors; photocatalyst; 2D group-VA materials



Citation: Li, H.; Yang, Z. Recent Progress in Synthesis and Photonic Applications of Two-Dimensional Bismuthene. *Appl. Sci.* **2023**, *13*, 6885. <https://doi.org/10.3390/app13126885>

Academic Editor: Antonio Di Bartolomeo

Received: 15 May 2023

Revised: 1 June 2023

Accepted: 3 June 2023

Published: 6 June 2023



Copyright: © 2023 by the authors. Licensee MDPI, Basel, Switzerland. This article is an open access article distributed under the terms and conditions of the Creative Commons Attribution (CC BY) license (<https://creativecommons.org/licenses/by/4.0/>).

1. Introduction

In recent years, two-dimensional (2D) elemental materials from group-VA (P, As, Sb, and Bi) have ignited increasing research interest in various of applications, including electronics, optoelectronics, energy related applications, spintronics, and biomedicine [1–7]. Unlike graphene, with its semi-metallic characteristics, 2D group-VA materials normally exhibit semiconducting characteristic with considerable bandgaps, making them favorable for electronic applications [8]. Among group-VA materials, phosphorene is the first, and up until now, the most-studied 2D candidate, attracting significant interest for use in many research fields, thanks to its high carrier mobility over $10,000 \text{ cm}^2\text{V}^{-1}\text{s}^{-1}$, its tunable direct bandgaps from 0.3 eV (bulk) to 2.0 eV (monolayer), and its unique in-plane anisotropic properties [9–11]. However, phosphorene suffers from low stability when exposed to air, which should be optimized before considering the development of practical applications [12,13]. Recently, other 2D group-VA materials (As, Sb, Bi), namely arsenene, antimonene, and bismuthene have come into the spotlight due to their intrinsic wide band gaps, high carrier mobility, and good stability, which avert the main drawbacks of phosphorene [4].

As the last and heaviest element in group VA, bulk bismuth (Bi) exhibits a semi-metallic feature, with a small effective mass, a large mean free path, remarkable light-matter interaction, and low carrier density [14–16]. A previous study showed that Bi exhibits strong intrinsic spin-orbit coupling and conductive surface states, making it desirable for spintronic applications [14]. In general, when the thickness is thinner than the Fermi wavelength, Bi will undergo a transition from semimetal to semiconductor due to the quantum confinement effect [17,18]. Moreover, 2D Bi has been reported to

possess unique surface states and band structures, demonstrating layer-dependent topological properties [17,19]. In 2017, Reis et al. successfully synthesized a graphene-like bismuthene film on top of a SiC substrate, showing a topological energy gap of 0.8 eV, which renewed the research interest in atomically thin Bi [20]. Since bismuthene exhibits a small band gap, a large nonlinear refraction index, and ultrahigh carrier mobility, the material is favorable for photonic applications such as broadband photodetectors [19,21,22], mode-locked lasers [18,23,24], and all-optical switching [25,26]. For example, Tang et al. demonstrated an ultrasensitive terahertz photodetector based on 2D bismuth. The strong photoresponse observed was attributed to the asymmetric scattering of topological surface states, which was stimulated by the localized surface plasmon-induced terahertz field. Furthermore, 2D bismuthene shows a large specific surface area, a hexagonal lattice structure, and high stability in air, making it suitable for photocatalytic applications [27–29]. In addition, the saturable absorption ability of bismuthene makes it applicable in Q-switched lasers. Recent study has reported a universal photo-redox catalyst based on few-layer bismuthene nanosheets, demonstrating arrested catalytic activity in an organic transformation under various reaction conditions [28]. Although the number of original research articles on bismuthene and its photonic applications has increased rapidly in recent years, to the best of our knowledge, there is currently no specific review article focusing on this area.

Herein, we present a comprehensive review of the recent progress in photonic applications based on 2D bismuthene. First, we will briefly outline the crystalline structure, electronic attributes, and nonlinear optical properties of bismuthene. Then, the common synthesis methods used to realize high quality bismuthene, from both top-down and bottom-up approaches, will be introduced. Next, we will review the typical photonic devices based on bismuthene, in the sequence of photodetectors, non-linear photonics devices, and photocatalytic applications. The performance and mechanisms of the devices will also be discussed. Finally, the review will be summarized, and some perspectives and future prospects of this field will be provided.

2. Structure and Properties of Bismuthene

Different from its bulk, bismuthene exhibits intriguing physical properties owing to the quantum confinement effect [30–32]. The crystalline structure and fundamental properties of 2D bismuth make it attractive for the development of photonic applications. In this section, the crystal structure, electronic structure, and nonlinear optical properties of bismuthene will be outlined.

2.1. Structure and Electronic Properties

According to the theoretical results of the first-principles calculation, bismuthene exhibits three possible phases, i.e., α -, β -, and ξ -phases, with comparable lowest average binding energy. However, until now, only α - and β -bismuthene have been successfully realized in the laboratory, owing to their energetic stability [15,33]. As shown in Figure 1a,b, α -phase bismuthene has a honeycomb, wrinkled crystal structure, and β -phase bismuthene possesses a crooked layered structure. Both α - and β -bismuthene exhibit a layered structure, with weak van der Waals (*vdWs*) interactions between adjacent layers, enabling the straightforward acquisition of bismuthene by the mechanical exfoliation method. It has been reported that α -phase bismuthene exhibits non-trivial 2D topological insulator properties, with a large bulk bandgap at room temperature [15]. Compared to the α -phase type, β -phase bismuthene is more stable, with the ability to sustain a pristine morphology and layer structure, even under temperatures up to 400 °C (Figure 1c) [34]. Moreover, because of the difference between the in-plane and out-of-plane inter-atomic distance, β -bismuthene shows clear anisotropic properties (12%). Excluding α -phase and β -phase bismuthene, bismuth atoms can also form buckled square or octagon rings, which have been confirmed by molecular dynamics calculations [35].

Previous theoretical studies based on the density functional theory (DFT) have been carried out to study the band structures of bismuthene for evaluating their electrical characteristics [36–38]. According to the computation results, α -bismuthene and β -bismuthene are direct bandgap semiconductors, with bandgaps of 0.36 eV and 0.99 eV, respectively (Figure 1d). In addition, the absorption coefficient of both α -bismuthene and β -bismuthene were higher than 10^4 cm^{-1} , and the high mobility of bismuthene (10^2 – $10^3 \text{ cm}^2/\text{V}\cdot\text{s}$) was obtained using the acoustic phonon limited mobility approach [39]. Furthermore, by employing HSE06 method to revise the band structure, β -bismuthene shows a new indirect band gap feature [37]. Meanwhile, the Rashba spin-splitting phenomenon was also observed in the valence band maximum states. The Rashba energy can be modulated by applying in-layer biaxial strain, owing to the buckling structure of β -bismuthene. Importantly, β -bismuthene can undergo a transition from indirect band gap to direct band gap, as well as from semiconducting to semimetallic characteristics by enforcing the biaxial strain. In addition to monolayer bismuthene, multi-layer bismuthene was also confirmed to demonstrate a transition from semiconductor to semimetallic [40].

2.2. Nonlinear Property

The nonlinear properties of bismuthene have attracted significant attention due to their ability to provide spin–orbit interaction, a high nonlinear refractive index, and semimetallic bonding [41,42]. The nonlinear optical properties of bismuthene have been investigated by the measurement of spatial self-phase modulation (SSPM) [24]. As shown in Figure 1e,f, the diffraction rings of 2D bismuth have been observed in the visible wave range. It should be noted that under different irradiation wavelengths of 532 nm and 633 nm, the number of diffraction rings all demonstrate a quasi-linearly increasing trend with an increase in laser power density. Meanwhile, the slope of the relationship between the ring numbers and light intensity decreases with increasing laser wavelength, indicating that the SSPM of bismuthene is caused by the electronic transition. The third-order nonlinear susceptibility (e.s.u.) of bismuthene was calculated by

$$\chi_{total} = \frac{c\lambda n_0}{2.4 \times 10^4 \pi^2 L_{eff}} \frac{dN}{dI}$$

where n_0 is the linear refractive index, λ is the wavelength, and L_{eff} is effective optical propagation length, respectively. It is worth noting that the third-order nonlinear susceptibility (e.s.u.) and nonlinear refractive ($10^{-6} \text{ cm}^2/\text{W}$) of bismuthene are much lower than those of 2D black phosphorus (BP) [43], revealing bismuthene as a suitable candidate for optical communication, as well as for all optical switching applications. In addition, the saturable absorption ability is also investigated. The saturation intensity at $1.5 \mu\text{m}$ is approximately equal to $30 \text{ MW}/\text{cm}^2$, and the modulation depth is up to 2.03%, respectively. By applying bismuthene as a saturable absorber, a mode-locked fiber laser was fabricated, demonstrating a large signal-to-noise ratio of up to 55 dB and a repetition rate of 8.83 MHz, which will be discussed in detail in subsequent sections of this review.

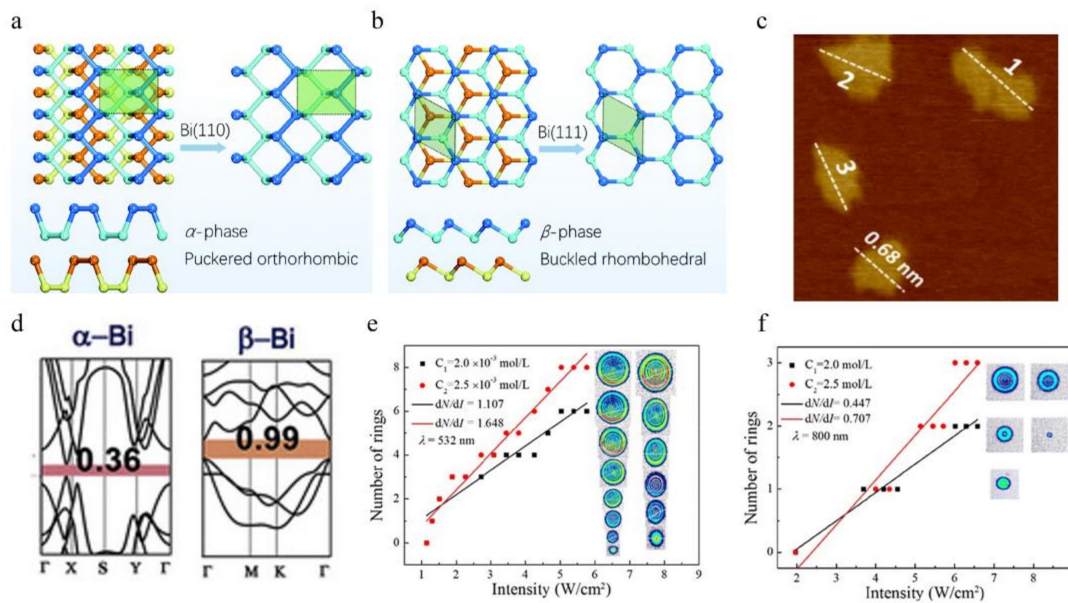


Figure 1. (a,b) Schematics of α -bismuthene and β -bismuthene from the top and side views [30]. (c) AFM image of β -bismuthene [34]. (d) Calculated band diagram of α - and β - bismuthene [44]. (e,f) The diffraction ring patterns and number of rings in the bismuthene solution under different powder intensities at illuminations of 532 nm and 633 nm, respectively [24].

3. Production of 2D Bismuthene

Effective fabrication methods to realize high quality bismuthene are the key to realizing devices with outstanding performance. It is well known that top-down and bottom-up methods are the two main strategies for synthesizing 2D materials. In general, the top-down strategy for fabricating 2D bismuth includes mechanical exfoliation, liquid-phase exfoliation, chemical exfoliation, etc. [45,46]. Common bottom-up fabrication methods include chemical vapor deposition (CVD) [22], pulsed laser deposition (PLD) [17], molecular beam epitaxy (MBE) [47], and electron beam (e-beam) evaporation [48]. In this section, several methods for the production of bismuthene will be described, and the advantages and drawbacks of each are also discussed.

3.1. Top-Down Approach

With the assistance of the proper chemical solvents and sonication processes, the interlayer *vdWs* force of bulk Bi can be broken to obtain 2D Bi nanosheets [24]. A typical convenient liquid exfoliation process is shown in Figure 2a. Bulk bismuth was ground into power using isopropyl alcohol. Subsequently, the bismuth isopropyl solution was subjected to both bath and probe sonication for 10 h, respectively. Next, 2D bismuthene was obtained after the centrifugation process. It should be noted that the type of chemical solvent used is of great significance for the efficient production of bismuthene nanosheets. The exfoliation efficiency can be optimized when the solvent's surface tension component ratios are comparable to those of bismuthene [49].

As an efficient and low-cost method, liquid exfoliation can fabricate high-quality Bi with high efficiency and yield [50]. The strong interaction between bulk Bi and a suitable solution (such as isopropyl alcohol) leads to the dispersion of the bismuth nanosheets in the solvent [51]. In 2019, Huang et al. exfoliated Bi nanosheets from Bi powder in an ethanol solution using sonication-assisted liquid exfoliation [50]. Few-layer Bi was prepared after 1 h of sonication at 950 W and centrifugation at 500 rpm. According to the atomic force microscope (AFM) image (Figure 2b), monolayer bismuth nanosheets were successfully fabricated. However, owing to defects in the exfoliation process, the exfoliated layers are not of high quality. In addition, the lateral size of the as-produced nanosheets ranges from

the nm scale to the multiple μm scale. The optimization of the exfoliation process in order to better control the size of the obtained samples should be addressed in the future.

In addition to the liquid exfoliation process, 2D Bi can also be fabricated by the electrochemical exfoliation method due to its high chemical durability and the low cost of bulk metallic Bi [52,53]. Thanks to the advantages of short production time, moderate fabrication conditions, and high yield, the electrochemical exfoliation method provides a favorable platform for the mass production of 2D nanosheets. When bismuthene is prepared using a standard electrochemical exfoliation method based on a DC voltage apparatus, bulk Bi works as the cathode, and platinum foil works as the anode. During the fabrication process, both are soaked in the proper organic solution. The exerted bias facilitates the insertion of cations between the molecular layers, which can effectively increase the inter-layer spacing. In 2019, 2D Bi, with a lattice fringe of 0.23 nm, was successfully exfoliated using a rapid electrochemical cathodic exfoliation method, resulting in Bi nanosheets with a large reactive surface area, beneficial for electrocatalytic performance (Figure 2c) [53]. Thanks to the significant field influence and the capacity to precisely tune the voltage, electrochemical exfoliation is an effective method to produce 2D Bi with good crystallinity and high yield [52,54]. However, owing to the introduction of organic solvents, the residues of the solution restrict the quality of the exfoliated samples.

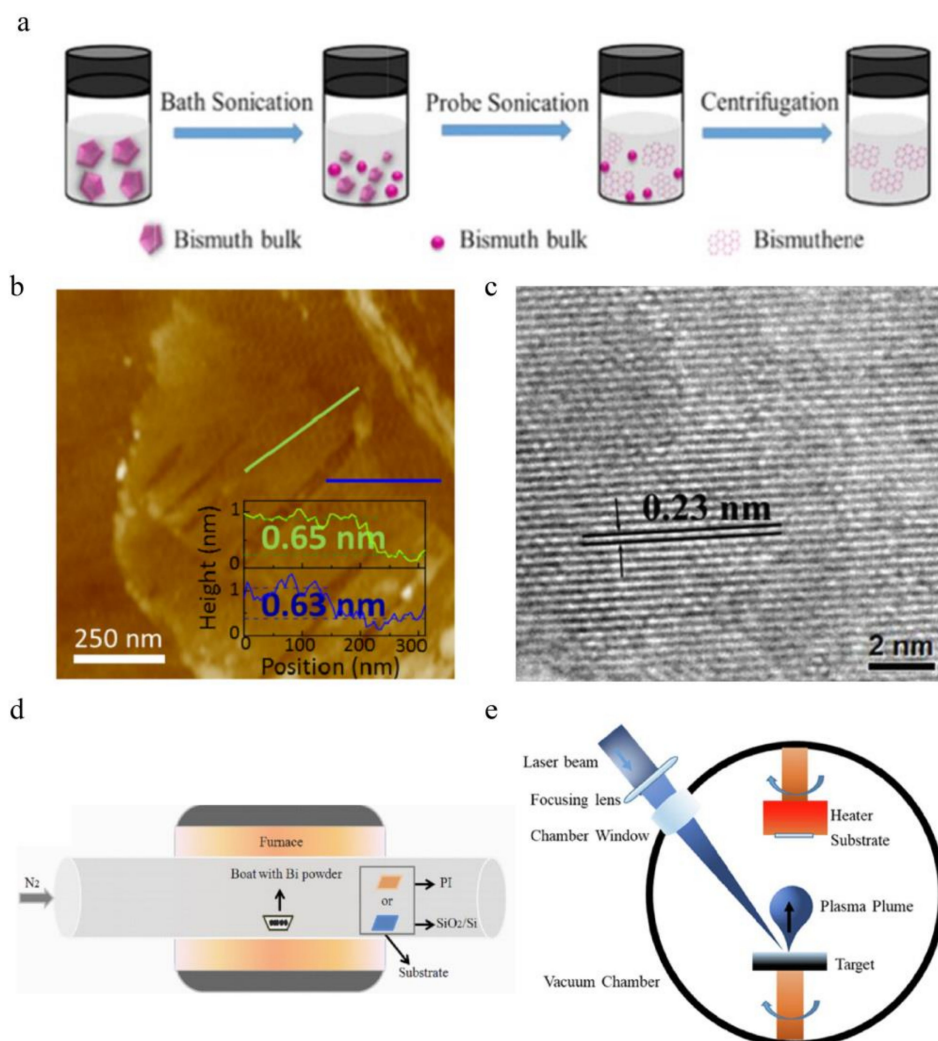


Figure 2. (a) Schematic diagram of the bismuthene liquid exfoliation process. [24]. (b) AFM image of the bismuthene layer [50]. (c) High resolution TEM image of the electrochemical exfoliated bismuth nanosheets [53]. (d) Schematic figure of the CVD process for preparing bismuthene [22]. (e) Schematic picture of the PLD system [55].

3.2. Bottom-Up Approach

In addition to the top-down methods, a series of bottom-up methods have also been utilized in the fabrication of 2D Bi layers. CVD is one of the most widely used bottom-up methods used to synthesize 2D materials. In 2020, Zhou et al. successfully grew 2D Bi films on both rigid (SiO_2/Si) and flexible (polyimide) substrates using CVD. As shown in Figure 2d, Bi powder in a silica boat is placed in the heating zone of the furnace. Using the flow of N_2 gas in the tube, the Bi film will form on the substrates, which are located downstream of the system [56]. The size and thickness of the CVD-grown 2D bismuth nanosheets can be controlled by tuning the key preparation parameters, such as reaction atmosphere, gas flow rate, processing temperature, and reaction time [57]. Over the last 5 years, Hu et al. have synthesized high quality Bi nanoflakes on Cu foil substrate using CVD. By introducing an h-BN top layer, the structural transformation of 2D Bi is effectively restricted. After removing the h-BN layer by mechanical exfoliation, 2D Bi nanoflakes show extraordinary thermal stability evidenced by the phenomenon of its ability to resist oxidation after annealing at 500 °C for 10 min. It is also significant that the obtained 2D Bi nanoflakes could be applied in electrochemical CO_2 reduction reactions, retaining high crystallinity beyond 15 h.

PLD is one of the most effective physical methods to synthesize large-scale 2D materials and heterostructures [55]. As shown in Figure 2e, during the PLD procedure, focused laser pulses strike the bulk target, and the generated energetic plasma plume is collected on a pre-heated substrate. In contrast to CVD, the processing temperature of 2D materials using PLD is usually relatively low. In addition, PLD exhibits the advantages of a high growth rate, better controllability of the film, and stoichiometric growth. In 2019, our group grew high crystallinity centimeter-scale Bi layers using PLD [17]. The 2D Bi(111) and Bi(110) thin films can be both produced by tuning the processing temperature at 100 °C and room temperature, respectively. The thickness of Bi(111) and Bi(110) can be precisely controlled by the number of laser pulses. Meanwhile, the large scale and uniform surface give PLD-grown bismuthene great potential for developing practical device applications [55].

MBE is another commonly used bottom-up method to synthesize high quality 2D films and nanostructures [58,59]. The preparation process is realized in an ultrahigh vacuum chamber, which could prevent contamination by impurities. MBE is suitable for producing large-scale films with a consistent thickness, and can be processed with several types of in situ characterization equipment, such as reflection high-energy electron diffraction (RHEED) systems, to monitor the fabrication process, which can rarely be achieved in other bottom-up methods. In order to synthesize bismuthene, bulk Bi is heated to sublimation in an MBE system, forming a 2D Bi thin film on the substrates [47,60]. By tuning the substrate temperature, different phases of bismuthene are synthesized [61]. For example, Nagao et al. have grown multiple-layer 2D Bi films on Si(111) substrate using MBE [62]. The ultrathin Bi films with a (012)-oriented phase were generated above the wetting layer. This bismuth structure, discovered for the first time, is similar to the teratoid phase of BP.

Besides PLD and MBE, e-beam evaporation is also feasible for the synthesis of 2D-layered Bi [48,63]. Table 1 shows the comparison of the growth conditions and the material quality of 2D materials obtained using different fabrication techniques. In summary, the bottom-up synthesis of bismuthene is a significant complement to the top-down methods. The successful realization of wafer-scale few- and mono-layer bismuth films builds a solid foundation for the future development of high-performance photonic applications based on bismuthene.

Table 1. Comparison of techniques to fabricate bismuthene.

	Size	Throughput	Thickness Homogeneity	Fabrication Rate	Processing Temperature	Refs
Liquid exfoliation	1–10 μm	High	Moderate	Moderate	RT	[24] [50]
Electrochemical exfoliation	1–10 μm	High	Moderate	Moderate	RT	[53]
CVD	Over 1 cm	High	Very High	Slow	High	[56]
PLD	Over 1 cm	High	High	Fast	Moderate	[17]
MBE		High	High	Slow	High	[61]

4. Photonic Applications Based on 2D Bismuth

Bismuthene has been applied in diverse photonic applications because of its narrow bandgaps, high carrier mobility, strong light response, and fine biocompatibility [4,24]. In this section, we provide a comprehensive overview regarding nonlinear photonic devices, photodetection devices, and photocatalytic applications based on 2D bismuth. The architecture, performance, and mechanisms of the devices will be illustrated and discussed in detail.

4.1. Nonlinear Photonic Devices

Recently, bismuthene has received significant attention for its potential use in saturable absorbers thanks to its unique electron mobility properties, spin-orbit coupling, and incredible stability in ambient conditions [20,23,64]. In 2018, Guo et al. first demonstrated a sub-200 fs soliton mode-locked fiber laser using bismuthene as the saturable absorber (Figure 3a) [16]. The self-started mode-locking laser process only occurred when the bismuthene-saturable absorber was located in the ring laser cavity. The 1561 nm stable soliton pulses with width as low as 193 fs were generated when the pump power increased from 100 mW to 350 mW. As shown in Figure 3b, symmetrically distributed Kelly sidebands can be observed in the output optical spectrum, which reveals the soliton state of the pulse. According to the 2 μ s-long soliton pulse trace on the oscilloscope (Figure 3c), the soliton pulse with a period of 113.4 ns and a frequency of 8.85 MHz is propagated in the laser cavity. Furthermore, the autocorrelation trace of the soliton pulse was also measured in the picosecond time scale. The extracted bandwidth is 193 fs, and the corresponding time-bandwidth product (TBP) is 0.342. Importantly, this soliton is almost perfect because the TBP of the device is similar to the theoretical limit (0.315). In addition, according to the radio frequency (RF) spectrum of the device, the peak of the soliton pulse is located at the repetition rate of 8.85 MHz with a signal-to-noise ratio of \sim 55 dB, which demonstrates the pulse with high stability. It is significant that both the pulse duration time (193 fs) and the output power (5.6 mW) of the device outperformed those of the antimonene microfiber-based laser, attributable to the better nonlinear ability of bismuthene [65]. Additionally, a passively mode-locked ytterbium-doped mode-locked fiber laser was constructed by using bismuthene as the saturable absorber, with modulation depth and saturation intensity of 2.4% and 0.3 MW/cm², respectively [23]. When the pump power was set at 122.1 mW, a single-pulse soliton molecule was generated, with a 621.5 fs pulse duration at a central wavelength of 1557.5 nm (Figure 3d), a spectral width of 10.35 nm, and a fundamental cavity repetition of 22.74 MHz (Figure 3e). In addition, by adjusting the pump power, the generated single molecules can react with each other. Owing to the outstanding nonlinear optical properties and semimetal characteristics of bismuthene, two-pulse, eight-pulse, and fourteen-pulse soliton molecules, with both tightly and loosely temporal separation, were observed for the first time. Over the last 5 years, Xu et al. have adopted a bismuthene nanosheet-saturable absorber to achieve harmonic dual-wavelength mode-locked picosecond pulses [66]. As shown in Figure 3f, the modulation depth (7.7%) and saturation intensity (16 MW/cm²) of bismuthene nanosheets at 1563 nm are obtained due to the enhanced light modulation ability [67]. The proposed nonlinear fiber laser can generate stable harmonic mode-locked pulses or harmonic dual-wavelength mode-locking pulses by adjusting the pump power.

In contrast to the previous research, Yang et al. not only characterized the modulation depth of bismuthene, but also studied the underlying mechanism of nonlinear saturable absorption, which is related to the excited-state dynamics [68]. As depicted in Figure 4a, the relaxation of photogenerated carriers is distributed through three channels, including rapid intraband (\sim 3 ps) carrier-carrier or carrier-phonon scattering, slower interband relaxation (\sim 420 ps), and the slowest trap state-mediated electro-hole recombination. This mechanism indicates the important role of intermediate states and the origin of saturable absorption. In addition, the fabricated mode-locked Tm-doped fiber laser successfully generates a 2030 nm pulse with maximum energy of 6.6 nJ, which is higher than that of the

graphene based device [69], suggesting that bismuthene is favorable for an optical fiber communication application.

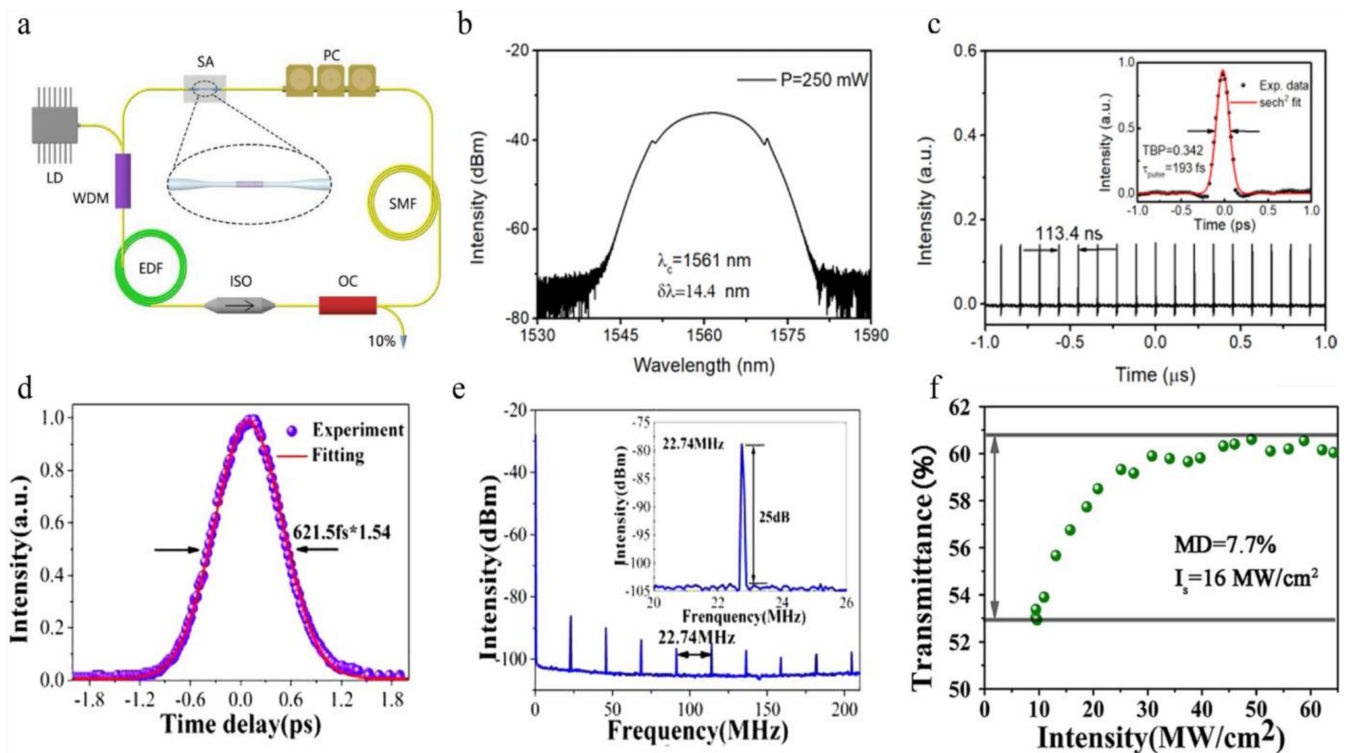


Figure 3. Schematic diagram and key parameters of the bismuthene-based laser. (a) Schematic figure of mode-locked fiber device based on the bismuthene saturable absorber. (b) Optical spectrum characteristic of the solution pulse at 250 mW. (c) Oscilloscope trace of solution pulse. The inset of the picture shows the autocorrelation trace of the pulse [16]. (d) The autocorrelation trace of the single conventional soliton. (e) The radio frequency spectrum of the generated single conventional solitons. (f) The transmission as a function of the average power of bismuthene nanosheets at 1563 nm [23].

Apart from generating mode-locked pulses, the bismuthene saturable absorber can also be used as a Q-switch in ultrafast lasers. In 2019, bismuthene was reportedly employed in a passively Q-switched fiber laser at the mid-infrared region (MIR) (Figure 4b) [70]. Owing to the broadband nonlinear optical response of bismuthene from the NIR to the MIR region, a 645 fs Er^{3+} -doped fiber laser was demonstrated, with a duration of 1.86 μ s and a signal-to-noise ratio of 37.8 dB at 2789 nm. Recently, Chen et al. grew a few-layer bismuthene nanosheet using the solution based method and demonstrate a passively Q-switched Nd: GYAP laser at 1300 nm [71]. Compared with the center wavelength of the continuous-wave laser, the passively Q-switched laser shows a blueshift center wavelength because of the insertion loss of the bismuthene saturable absorber (Figure 4c). In addition, it was discovered that the peak power and pulse width of the bismuthene-based laser both outperform those of the passively Q-switched laser using MoSe_2 [72] or ReS_2 [73] as saturable absorbers. In 2019, Feng et al. successfully fabricated bismuthene with a modulation depth as high as 22.1% and a saturation fluency of 21.5 $\mu\text{J}/\text{cm}^2$ [74]. The 880 nm pumped Nd:BGO passively Q-switched laser can produce a stable laser beam with a repetition rate of up to 223.7 kHz and a duration down to 256 ns (Figure 4d). Table 2 summarizes the main figures of merit (FOMs) of the lasers based on bismuthene and other 2D materials. It can be determined that the bismuthene-based lasers exhibit output power and single pulse energy superior to those of other commonly studied 2D candidates. The outstanding performance of the lasers may be attributed to the excellent nonlinear property of bismuthene, which could pave the way for potential applications such as optical communication and laser materials processing.

Table 2. FOMs of lasers based on bismuthene and other 2D materials.

2D Materials	λ_c [nm]	Pulse Width [fs]	Output Power [mW]	Single Pulse Energy [nJ]	f_{rep} [MHz]	Refs
Bismuthene	1561	193	5.6		8.85	[16]
Bismuthene	1557.5	621.5	122.1		22.74	[23]
Bismuthene	2789	645				[70]
Bismuthene	1065	2.56×10^5		590	0.2237	[74]
Antimonene	1557.7	552	0.66	6.43×10^{-2}	~25	[65]
BP	1532	940	5.6		4.69	
MoS ₂	1042.6	6.56×10^5	2.37	0.35	6.74	[75]
MoTe ₂	1559.5	229	57	2.14	26.601	[76]
WS ₂	1561	246	18	0.178	80	[77]
SnS ₂	1562	623	1.2	4.09×10^{-2}	29.33	[78]
MoSe ₂	1340	4.2×10^5	52.6		238	[72]
ReS ₂	1300	4.03×10^5		420	0.214	[73]
Bi ₂ Se ₃	1571	579	1.56	0.112	12.54	[79]
TiS ₂	1544.5	402			~5.7	[80]

Thanks to its layer-dependent bandgaps, strong light-matter interaction ability, and good air-stability, bismuthene can also be used in designing nonlinear optical signal processing systems. Recently, Wang et al. constructed, for the first time, an all-optical signal processing fiber system based on bismuthene-coated fiber [25]. Thanks to the strong light-matter interaction of bismuthene, the optical fiber system can not only be used as an optical Kerr switch, but it also operates as a four-wave-mixing (FWM) wavelength converter (Figure 4e). In 2017, Lu et al. realized all optical switching based on the spatial cross phase modulation of bismuthene owing to its strong nonlinear optical absorption and the refraction effect [26]. The 532 nm switching laser and 633 nm signal laser were injected into bismuthene to obtain a high modulation depth and all optical switching. According to the generated diffraction rings (Figure 4f), the switched light and signal light were generated simultaneously. It can be determined that the variation of rings is strongly dependent on the switching light. In addition, the authors also indicated that the modulation depth can be adjusted by regulating the energy of the switched light, which is suitable for the fabrication of nonlinear photonics devices, such as the passively Q-switched and light modulators.

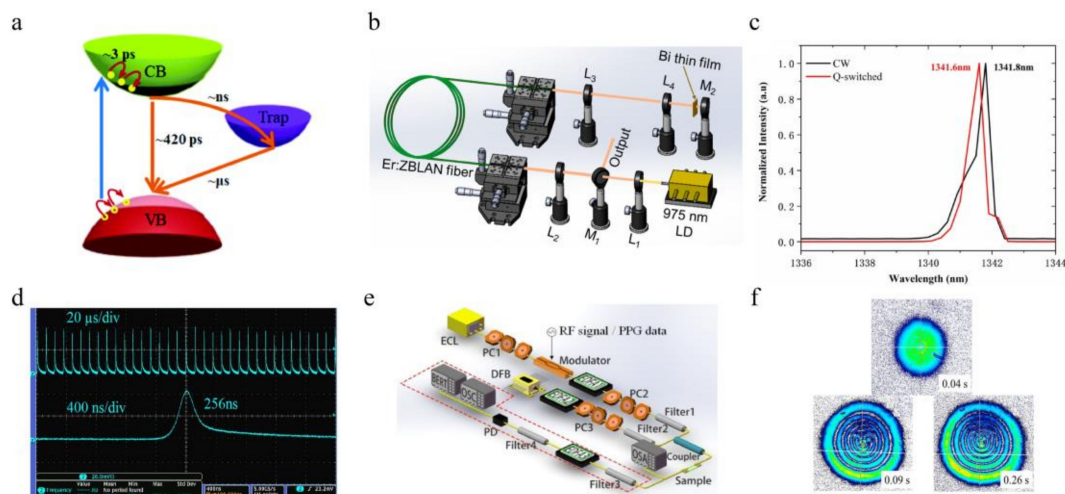


Figure 4. Schematic diagram and key parameters of the bismuthene-based nonlinear devices. (a) Schematic figure showing the bismuthene band structure in the trap state [68]. (b) Schematic figure of the passively Q-switched laser with the bismuthene saturable absorber [70]. (c) Optical spectrum of the continuous-wave laser and the passively Q-switched laser, respectively [71]. (d) Q-switched pulses recorded at 400 ns/div and 20 μs/div [74]. (e) Schematic graphic of the FWM setup based on bismuthene-coated microfiber [25]. (f) The formation process of the diffraction rings of the 633 nm laser corresponding with the 532 nm laser excitation [26].

4.2. Photocatalysis

The 2D bismuthene has been widely used in photocatalysis applications due to its high carrier mobility [81], tunable band structure [47], and low toxicity [45]. Very recently, Melek et al. demonstrated that 2D bismuth was used as an efficient photocatalyst in the liquid-phase organic transformation, with high product yield [28]. In this work, furan 1a and 4-chlorobenzenediazonium salt 2a were chosen as compounds for the investigation of photocatalytic activity in the photoredox C-H arylation. During the process, the excited electrons of bismuthene are transferred to the aryl diazonium salt and result in the aryl radical. Compared to sole bismuthene, the compound of diazonium salt 2a and bismuthene shows photoluminescence (PL) spectra, with largely decreasing intensity. The phenomenon can be explained by the rapid migration of photocarriers in bismuthene because the average lifetime of the carriers of bismuthene in diazonium salts is much larger than that of sole 2D bismuth (Figure 5a). Thanks to the narrow bandgap of bismuthene, the carrier excitation can occur without external incentives. Therefore, unlike other photocatalyst that require additional conditions to catalyze the C-H arylation of (hetero)arenes, bismuthene can operate at a low temperature ($-15\text{ }^{\circ}\text{C}$), without utilizing a light source, as well as under dark conditions. Moreover, it is also of note that, unlike other photocatalysts, the reaction process operates normally without complicated equipment, precise environments, or specific light sources [82,83]. Additionally, bismuthene can not only catalyze C-H arylation with aryl diazonium, but also with other heteroarenes such as furan, thiophene, and pyrrole, which allows the bismuthene to be used in diverse applications [84].

In 2021, Zhang et al. inserted 2D Bi into $\text{C}_3\text{N}_4/\text{BiOCl}$ to form a 2D/2D/2D heterostructure photocatalyst, in which bismuthene acts as an effective metal electron mediator (Figure 5b) [27]. As shown in Figure 5c, the type of heterojunction is changed from type-II to the Z-scheme. The tunneling effect of the bismuthene layer promotes the combination of photogenerated electrons in C_3N_4 , with holes in the valence band of BiOCl, significantly improving the efficiency of the photocatalytic reaction. The CH_4/CO yield of the $\text{C}_3\text{N}_4/\text{bismuthene}/\text{BiOCl}$ heterostructure is up to $61/71\ \mu\text{molg}^{-1}\text{h}^{-1}$, which is superior to that of the other reported Bi-based photocatalysts [85–87]. Apart from carbon dioxide reduction, the bismuthene-based heterostructure can also be applied in other photocatalysis reactions. Very recently, Ge et al. reported that the InTe/bismuthene heterostructure can produce hydrogen from water splitting, achieving a maximum solar-to-hydrogen conversion efficiency (η_{STH}) up to 16.17% under 9% strain (Figure 5d) [88]. Compared to monolayer InTe nanosheets, the combination with bismuthene can strongly increase the efficiency of the hydrogen evolution reaction (HER). Meanwhile, the variation of Gibbs free energy verifies the feasibility of the thermodynamics of the HERs using the InTe/bismuthene heterojunction.

4.3. Photodetectors

Thanks to its narrow bandgaps, high carrier mobility, and strong absorption ability, bismuthene shows great potential for use in high performance photodetection applications [21,89,90]. In 2020, Zhou et al. designed photodetectors based on 2D bismuth thin films on both rigid (SiO_2/Si) and flexible (PI) substrates using vapor deposition [22]. The 2D Bi photodetectors on SiO_2/Si not only showed a broadband photoresponse from 405 to 1064 nm, but also exhibited a self-powered, stable photodetection performance. According to Figure 6a, the 2D Bi layer on top of the device plays the role of a light absorption layer and a surface conductive channel due to its topological nature and its high carrier mobility. Some carriers prefer to transfer along the surface Bi channel because the thickness of the Bi layer is less than one mean free path, which is beneficial for photocurrent generation and quick response time (14 ms). Additionally, the Bi film on the PI substrates also showed similar photoresponse and demonstrated outstanding durability and reproducibility by bending the devices with different curvature radiuses. More recently, Wang et al. fabricated a photoelectrochemical (PEC) photodetector based on 2D bismuth nanosheets by utilizing a solid electrolyte prepared using polyvinyl alcohol (PVA) (Figure 6b) [91]. By using a

solid electrolyte instead of a traditional liquid electrolyte, the volume of the photodetectors will be reduced and the electrolyte leakage problem can be addressed during the folding process. As shown in Figure 6c, the heterojunction of 2D Bi nanosheets and the solid electrolyte will generate a built-in electric field, which could increase the separation efficiency of electron-hole pairs and enable the self-powered photodetection capability. In addition, the 2D Bi PEC photodetector was also fabricated on indium-tin oxide (ITO) substrate for designing a flexible and transparent photodetector. As shown in Figure 6d, the photocurrent remains at a steady value after bending 120 times, further verifying the excellent stability of 2D Bi-based flexible photodetection devices. Besides, the responsivity of photodetectors can be calculated using the following equation:

$$R_{\lambda} = I_{ph}/P_{\lambda}S$$

where R_{λ} stands for the photoresponsivity, I_{ph} represents the photocurrent of the photodetectors, P_{λ} is the incident power of the illumination, and S represents the effective illumination area. Thus, the obtained responsivity of Bi photodetectors is up to $9.7 \mu\text{A}/\text{W}$, which is superior to that of a BP ($5.4 \mu\text{A}/\text{W}$)-based PEC-type photodetector under similar circumstance [92].

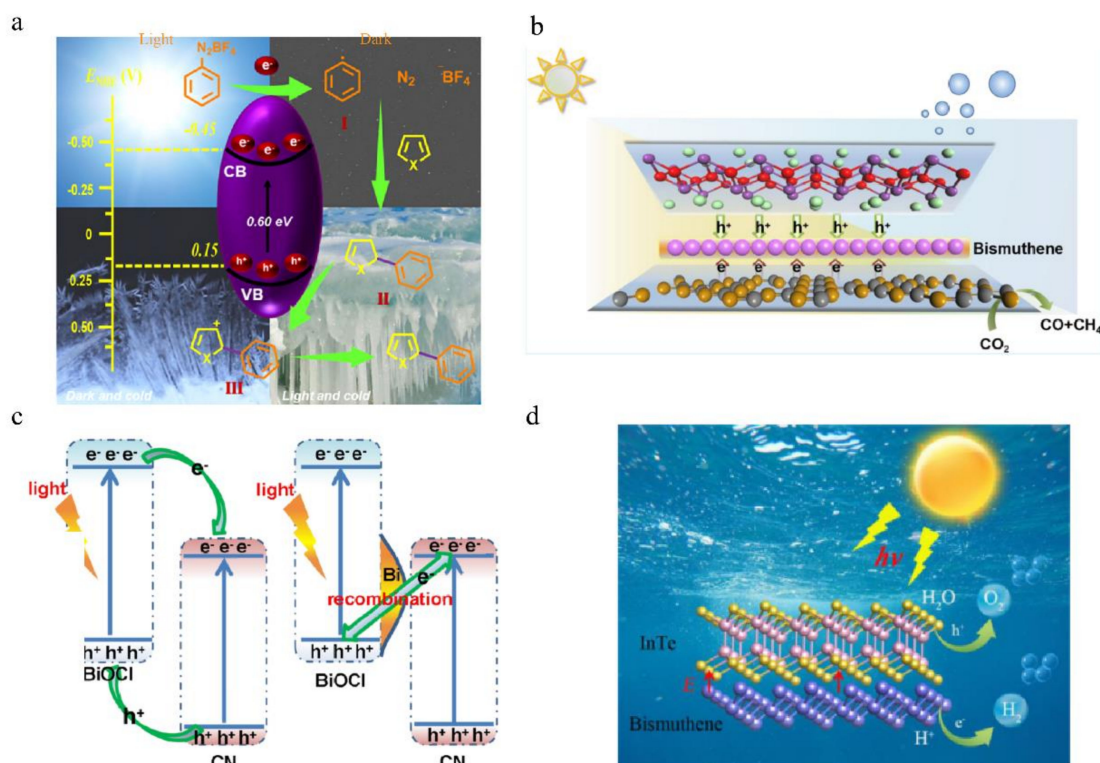


Figure 5. Schematic diagram and mechanisms of Bi-based photocatalyst. (a) Catalytic process of bismuthene photoredox C-H arylation of (hetero)arenes [28]. (b) Schematic figure of the bismuthene photocatalytic CO_2 reduction reaction process. (c) Schematic picture of the charge transformations of the type-II $\text{C}_3\text{N}_4/\text{BiOCl}$ heterostructure and the Z-scheme $\text{C}_3\text{N}_4/\text{bismuthene}/\text{BiOCl}$ heterostructure [29]. (d) Schematic figure of the catalytic process of water splitting [88].

In the wake of improving the performance of the Bi detector, the strategy of combining 2D Bi with other materials to form heterostructure has garnered significant interest. Yao et al. demonstrated a $\text{Bi}/\text{WS}_2/\text{Si}$ mixed dimensional heterostructure-based photodetector with outstanding photosensitivity up to $1.4 \times 10^8 \text{ cm}^2/\text{W}$ [93]. As illustrated in Figure 6e, the photogenerated carriers of Si are unable to tunnel into the Bi layer owing to the wide blocking barrier induced by the WS_2 layer. This phenomenon could effectively weaken the recombination efficiency of the generated carriers. In addition, the WS_2

dangling-bonds-free surface passivates the surface of Si, which leads to the small surface state. Therefore, Bi/WS₂/Si possesses fewer dangling-bonds compared to Bi/Si, which reduces the recombination loss. By utilizing such a structure, the separation of carriers and light absorption are more effective than those of Bi/Si, leading to the detectivity of up to 1.36×10^{13} Jones, which outperforms TMDs-based photodetectors [94–96]. Furthermore, the detectivity of the device maintains a constant value of 10^{10} Jones under different external biases (Figure 6f), which can be explained by the equally balanced trade-off between the photocurrent and the dark current.

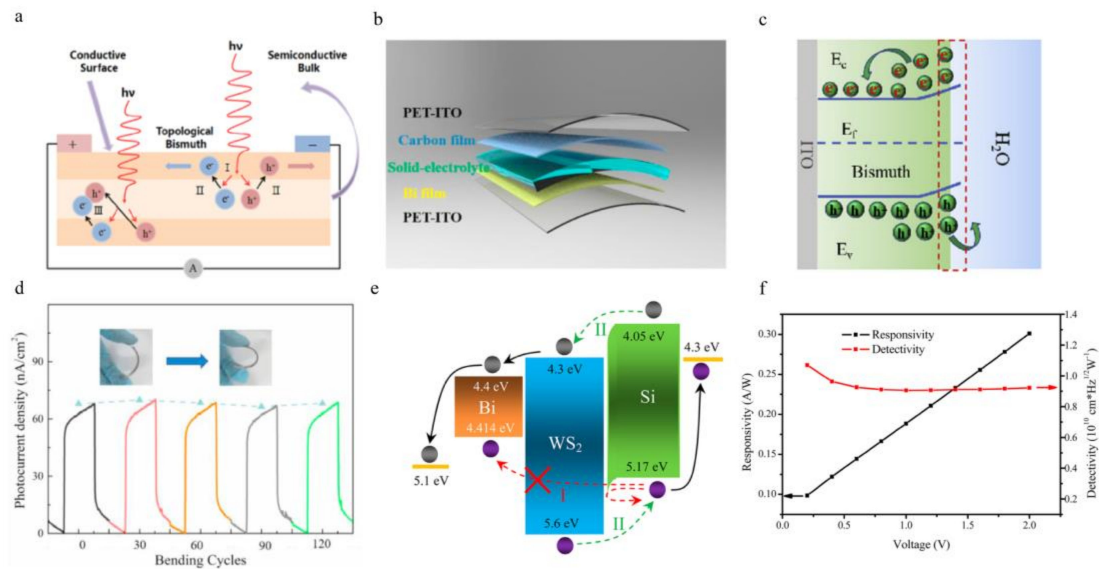


Figure 6. Schematic diagram and key parameters of the Bi-based photodetector. (a) Schematic figure of the working mechanism of Bi/Si under illumination [22]. (b) Schematic figure of the flexible PEC-type photodetector based on 2D Bi. (c) Band diagram of Bi nanosheets. (d) Photocurrent density of the PEC-type Bi-based device as a function of bending cycles [91]. (e) Band diagram of Bi/WS₂/Si heterostructure. (f) Detectivity and responsivity of Bi/WS₂/Si-based photodetector as a function of wavelength, respectively [93].

5. Conclusions and Outlook

Recent 2D bismuthene research progress has generated significant interest in exploring its features and potential applications. The atomically thin nature and layered structure of 2D bismuthene endow it with beneficial properties distinctive from its bulk. Bismuthene's layer-dependent optical band gaps, high carrier mobility, and excellent stability in air make it suitable for applications in both electronics and optoelectronics. In this review, we summarize the recent advances in photonic applications based on 2D bismuthene. The crystalline and electronic structure, as well as the nonlinear properties, of bismuthene are first reviewed, demonstrating a non-trivial 2D topological insulator and a suitable saturable absorption ability. Next, the techniques commonly used to realize bismuthene are outlined from both a top-down and bottom-up approach. A variety of photonic devices based on bismuthene are then discussed, including photodetectors, ultrafast photonic applications, and photocatalysts, each exhibiting attractive performance and great potential for modern photonic technologies. It is worth noting that bismuthene-based lasers exhibit a shorter pulse width than those of other 2D materials. Meanwhile, the responsivity and response time are comparable to those of graphene or TMDs-based heterostructures. Therefore, bismuthene is desirable for designing high performance photonic devices.

Currently, the design and device demonstration of bismuthene are still in the initial stages. Although the research has already achieved considerable progress, some challenges and opportunities for approaching the creation of practical devices remain:

1. The large-area synthesis method is one of the significant prerequisites for integrating 2D materials into practical applications. As we introduced in the article, the primary methods for the scalable growth of 2D bismuthene are mainly carried out by bottom-up techniques, including CVD, PLD, MBE, etc. However, currently, the low crystallinity and large number of defects of the obtained bismuthene limit its application in photonic and optoelectronic devices. Meanwhile, the poor controllability of the fabrication process, its slow growth rate, and its current high cost does not meet the criteria for commercialization. Therefore, developing a direct-synthesis method for realizing high quality 2D bismuthene films would be a high priority.
2. During the photocatalytic experiments, 2D bismuthene is easily oxidized to amorphous bismuth oxide due to its atomically thin nature and semimetal features, which will degrade the efficiency of photocatalysts. Thus, it is a crucial to discover a method to solve the oxidation issue of 2D Bi. A straightforward approach is to package the bismuthene into porous materials, which could reduce its exposure to oxidizing conditions. Another possible method is to integrate bismuthene photocatalysts into a photoelectrochemical system, which may also prevent the oxidation of 2D Bi.
3. Thanks to the weak vdWs interaction between the adjacent layers and the dangling-bond-free surface, 2D materials can form heterostructures by combining with another 2D candidate, or even materials of different dimensionality, which greatly expand the properties, functionalities, and applications of the 2D family. Considering the tunable band alignment and the combination of merits from different materials, 2D bismuthene heterostructures provide new strategies for designing high performance photonic applications. Moreover, the large contact surface and highly exposed surface atoms would create a bismuthene heterostructure with a large internal electric field, which is beneficial for photocatalytic activity. Thus, further exploration of the photonic and photocatalytic applications of 2D bismuthene heterostructures is highly desirable.

Author Contributions: Conceptualization, H.L. and Z.Y.; methodology, H.L. and Z.Y.; software, H.L. and Z.Y.; validation, H.L. and Z.Y.; formal analysis, H.L. and Z.Y.; investigation, H.L. and Z.Y.; resources, H.L. and Z.Y.; data curation, H.L. and Z.Y.; writing—original draft preparation, H.L. and Z.Y.; writing—review and editing, H.L. and Z.Y.; supervision, Z.Y.; project administration, Z.Y.; funding acquisition, Z.Y. All authors have read and agreed to the published version of the manuscript.

Funding: This research was funded by the National Natural Science Foundation of China, grant number 62105236.

Institutional Review Board Statement: Not applicable.

Informed Consent Statement: Not applicable.

Data Availability Statement: Not applicable.

Conflicts of Interest: The authors declare no conflict of interest.

References

1. Zhang, D.C.; Zhang, A.X.; Guo, S.D.; Duan, Y.F. Thermoelectric properties of beta-As, Sb and Bi monolayers. *RSC Adv.* **2017**, *7*, 24537–24546. [[CrossRef](#)]
2. Gui, R.J.; Jin, H.; Sun, Y.J.; Jiang, X.W.; Sun, Z.J. Two-dimensional group-VA nanomaterials beyond black phosphorus: Synthetic methods, properties, functional nanostructures and applications. *J. Mater. Chem. A* **2019**, *7*, 25712–25771. [[CrossRef](#)]
3. Zhang, S.L.; Guo, S.Y.; Chen, Z.F.; Wang, Y.L.; Gao, H.J.; Gomez-Herrero, J.; Ares, P.; Zamora, F.; Zhu, Z.; Zeng, H.B. Recent progress in 2D group-VA semiconductors: From theory to experiment. *Chem. Soc. Rev.* **2018**, *47*, 982–1021. [[CrossRef](#)] [[PubMed](#)]
4. Pumera, M.; Sofer, Z. 2D Monoelemental Arsenene, Antimonene, and Bismuthene: Beyond Black Phosphorus. *Adv. Mater.* **2017**, *29*, 1605299. [[CrossRef](#)]
5. Bhakhar, S.A.; Patel, N.F.; Zankat, C.K.; Tannarana, M.; Solanki, G.K.; Patel, K.D.; Pathak, V.M.; Pataniya, P. Sonochemical exfoliation and photodetection properties of MoS₂ Nanosheets. *Mater. Sci. Semicond. Process.* **2019**, *98*, 13–18. [[CrossRef](#)]
6. Pataniya, P.; Zankat, C.K.; Tannarana, M.; Sumesh, C.K.; Narayan, S.; Solanki, G.K.; Patel, K.D.; Pathak, V.M.; Jha, P.K. Paper-Based Flexible Photodetector Functionalized by WSe₂ Nanodots. *ACS Appl. Nano Mater.* **2019**, *2*, 2758–2766. [[CrossRef](#)]

7. Bansal, S.; Das, A.; Jain, P.; Prakash, K.; Sharma, K.; Kumar, N.; Sardana, N.; Gupta, N.; Kumar, S.; Singh, A.K. Enhanced Optoelectronic Properties of Bilayer Graphene/HgCdTe-Based Single- and Dual-Junction Photodetectors in Long Infrared Regime. *IEEE Trans. Nanotechnol.* **2019**, *18*, 781–789. [[CrossRef](#)]
8. Li, H.R.; Yang, Z.B. Recent progress in mid-infrared photodetection devices using 2D/nD (n = 0, 1, 2, 3) heterostructures. *Mater. Des.* **2023**, *225*, 111446. [[CrossRef](#)]
9. Liu, H.; Du, Y.C.; Deng, Y.X.; Ye, P.D. Semiconducting black phosphorus: Synthesis, transport properties and electronic applications. *Chem. Soc. Rev.* **2015**, *44*, 2732–2743. [[CrossRef](#)] [[PubMed](#)]
10. Ling, X.; Wang, H.; Huang, S.X.; Xia, F.N.; Dresselhaus, M.S. The renaissance of black phosphorus. *Proc. Natl. Acad. Sci. USA* **2015**, *112*, 4523–4530. [[CrossRef](#)]
11. Yang, Z.B.; Hao, J.H. Recent Progress in Black-Phosphorus-Based Heterostructures for Device Applications. *Small Methods* **2018**, *2*, 1700296. [[CrossRef](#)]
12. Yang, Z.B.; Hao, J.H.; Yuan, S.G.; Lin, S.H.; Yau, H.M.; Dai, J.Y.; Lau, S.P. Field-Effect Transistors Based on Amorphous Black Phosphorus Ultrathin Films by Pulsed Laser Deposition. *Adv. Mater.* **2015**, *27*, 3748–3754. [[CrossRef](#)] [[PubMed](#)]
13. Favron, A.; Gaufres, E.; Fossard, F.; Phaneuf-L'Heureux, A.L.; Tang, N.Y.W.; Levesque, P.L.; Loiseau, A.; Leonelli, R.; Francoeur, S.; Martel, R. Photooxidation and quantum confinement effects in exfoliated black phosphorus. *Nat. Mater.* **2015**, *14*, 826–832. [[CrossRef](#)] [[PubMed](#)]
14. Ning, W.; Kong, F.Y.; Xi, C.Y.; Graf, D.; Du, H.F.; Han, Y.Y.; Yang, J.Y.; Yang, K.; Tian, M.L.; Zhang, Y.H. Evidence of Topological Two-Dimensional Metallic Surface States in Thin Bismuth Nanoribbons. *ACS Nano* **2014**, *8*, 7506–7512. [[CrossRef](#)]
15. Lu, Y.H.; Xu, W.T.; Zeng, M.G.; Yao, G.G.; Shen, L.; Yang, M.; Luo, Z.Y.; Pan, F.; Wu, K.; Das, T.; et al. Topological Properties Determined by Atomic Buckling in Self-Assembled Ultrathin Bi(110). *Nano Lett.* **2015**, *15*, 80–87. [[CrossRef](#)] [[PubMed](#)]
16. Guo, B.; Wang, S.H.; Wu, Z.X.; Wang, Z.X.; Wang, D.H.; Huang, H.; Zhang, F.; Ge, Y.Q.; Zhang, H. Sub-200 fs soliton mode-locked fiber laser based on bismuthene saturable absorber. *Opt. Express* **2018**, *26*, 22750–22760. [[CrossRef](#)]
17. Yang, Z.B.; Wu, Z.H.; Lyu, Y.X.; Hao, J.H. Centimeter-scale growth of two-dimensional layered high-mobility bismuth films by pulsed laser deposition. *Infomat* **2019**, *1*, 98–107. [[CrossRef](#)]
18. Guo, P.L.; Li, X.H.; Feng, T.C.; Zhang, Y.; Xu, W.X. Few-Layer Bismuthene for Coexistence of Harmonic and Dual Wavelength in a Mode-Locked Fiber Laser. *ACS Appl. Mater. Interfaces* **2020**, *12*, 31757–31763. [[CrossRef](#)] [[PubMed](#)]
19. Yao, J.D.; Shao, J.M.; Yang, G.W. Ultra-broadband and high-responsive photodetectors based on bismuth film at room temperature. *Sci. Rep.* **2015**, *5*, 12320. [[CrossRef](#)]
20. Reis, F.; Li, G.; Dudy, L.; Bauernfeind, M.; Glass, S.; Hanke, W.; Thomale, R.; Schafer, J.; Claessen, R. Bismuthene on a SiC substrate: A candidate for a high-temperature quantum spin Hall material. *Science* **2017**, *357*, 287–290. [[CrossRef](#)]
21. Huang, H.; Ren, X.H.; Li, Z.J.; Wang, H.D.; Huang, Z.Y.; Qiao, H.; Tang, P.H.; Zhao, J.L.; Liang, W.Y.; Ge, Y.Q.; et al. Two-dimensional bismuth nanosheets as prospective photo-detector with tunable optoelectronic performance. *Nanotechnology* **2018**, *29*, 235201. [[CrossRef](#)] [[PubMed](#)]
22. Zhou, Q.Q.; Lu, D.L.; Tang, H.; Luo, S.W.; Li, Z.Q.; Li, H.X.; Qi, X.; Zhong, J.X. Self-Powered Ultra-Broadband and Flexible Photodetectors Based on the Bismuth Films by Vapor Deposition. *ACS Appl. Electron. Mater.* **2020**, *2*, 1254–1262. [[CrossRef](#)]
23. Wang, C.; Wang, L.; Li, X.H.; Luo, W.F.; Feng, T.C.; Zhang, Y.; Guo, P.L.; Ge, Y.Q. Few-layer bismuthene for femtosecond soliton molecules generation in Er-doped fiber laser. *Nanotechnology* **2019**, *30*, 025204. [[CrossRef](#)] [[PubMed](#)]
24. Lu, L.; Liang, Z.M.; Wu, L.M.; Chen, Y.X.; Song, Y.F.; Dhanabalan, S.C.; Ponraj, J.S.; Dong, B.Q.; Xiang, Y.J.; Xing, F.; et al. Few-layer Bismuthene: Sonochemical Exfoliation, Nonlinear Optics and Applications for Ultrafast Photonics with Enhanced Stability. *Laser Photonics Rev.* **2018**, *12*, 1700221. [[CrossRef](#)]
25. Wang, K.; Zheng, J.L.; Huang, H.; Chen, Y.X.; Song, Y.F.; Ji, J.H.; Zhang, H. All-optical signal processing in few-layer bismuthene coated microfiber: Towards applications in optical fiber systems. *Opt. Express* **2019**, *27*, 16798–16811. [[CrossRef](#)]
26. Lu, L.; Wang, W.H.; Wu, L.M.; Jiang, X.T.; Xiang, Y.J.; Li, J.Q.; Fan, D.Y.; Zhang, H. All-Optical Switching of Two Continuous Waves in Few Layer Bismuthene Based on Spatial Cross-Phase Modulation. *ACS Photonics* **2017**, *4*, 2852–2861. [[CrossRef](#)]
27. Zhang, D.T.; Cui, X.Q.; Liu, L.L.; Xu, Y.C.; Zhao, J.X.; Han, J.H.; Zheng, W.T. 2D Bismuthene Metal Electron Mediator Engineering Super Interfacial Charge Transfer for Efficient Photocatalytic Reduction of Carbon Dioxide. *ACS Appl. Mater. Interfaces* **2021**, *13*, 21582–21592. [[CrossRef](#)]
28. Ozer, M.S.; Eroglu, Z.; Yalin, A.S.; Kilic, M.; Rothlisberger, U.; Metin, O. Bismuthene as a versatile photocatalyst operating under variable conditions for the photoredox C-H bond functionalization. *Appl. Catal. B-Environ.* **2022**, *304*, 120957. [[CrossRef](#)]
29. Yue, C.L.; Zhu, L.L.; Qiu, Y.X.; Du, Z.L.; Qiu, J.L.; Liu, F.Q.; Wang, F.H. Recent advances of plasmonic elemental Bi based photocatalysts in environmental remediation and energy conversion. *J. Clean. Prod.* **2023**, *392*, 136017. [[CrossRef](#)]
30. Liu, X.H.; Zhang, S.L.; Guo, S.Y.; Cai, B.; Yang, S.Y.A.; Shan, F.K.; Pumera, M.; Zeng, H.B. Advances of 2D bismuth in energy sciences. *Chem. Soc. Rev.* **2020**, *49*, 263–285. [[CrossRef](#)]
31. Derakhshi, M.; Daemi, S.; Shahini, P.; Habibzadeh, A.; Mostafavi, E.; Ashkarran, A.A. Two-Dimensional Nanomaterials beyond Graphene for Biomedical Applications. *J. Funct. Biomater.* **2022**, *13*, 27. [[CrossRef](#)] [[PubMed](#)]
32. He, J.S.; Tao, L.L.; Zhang, H.; Zhou, B.; Li, J.B. Emerging 2D materials beyond graphene for ultrashort pulse generation in fiber lasers. *Nanoscale* **2019**, *11*, 2577–2593. [[CrossRef](#)] [[PubMed](#)]
33. Scott, S.A.; Kral, M.V.; Brown, S.A. A crystallographic orientation transition and early stage growth characteristics of thin Bi films on HOPG. *Surf. Sci.* **2005**, *587*, 175–184. [[CrossRef](#)]

34. Yang, F.; Elnabawy, A.O.; Schimmenti, R.; Song, P.; Wang, J.W.; Peng, Z.Q.; Yao, S.; Deng, R.P.; Song, S.Y.; Lin, Y.; et al. Bismuthene for highly efficient carbon dioxide electroreduction reaction. *Nat. Commun.* **2020**, *11*, 1088. [[CrossRef](#)]
35. Ersan, F.; Akturk, E.; Ciraci, S. Stable single-layer structure of group-V elements. *Phys. Rev. B* **2016**, *94*, 245417. [[CrossRef](#)]
36. Guo, Y.; Pan, F.; Ye, M.; Sun, X.T.; Wang, Y.Y.; Li, J.Z.; Zhang, X.Y.; Zhang, H.; Pan, Y.Y.; Song, Z.G.; et al. Monolayer Bismuthene-Metal Contacts: A Theoretical Study. *ACS Appl. Mater. Interfaces* **2017**, *9*, 23128–23140. [[CrossRef](#)] [[PubMed](#)]
37. Liu, M.Y.; Huang, Y.; Chen, Q.Y.; Li, Z.Y.; Cao, C.; He, Y. Strain and electric field tunable electronic structure of buckled bismuthene. *RSC Adv.* **2017**, *7*, 39546–39555. [[CrossRef](#)]
38. Kecik, D.; Ozcelik, V.O.; Durgun, E.; Ciraci, S. Structure dependent optoelectronic properties of monolayer antimonene, bismuthene and their binary compound. *Phys. Chem. Chem. Phys.* **2019**, *21*, 7907–7917. [[CrossRef](#)]
39. Qiao, J.S.; Kong, X.H.; Hu, Z.X.; Yang, F.; Ji, W. High-mobility transport anisotropy and linear dichroism in few-layer black phosphorus. *Nat. Commun.* **2014**, *5*, 4475. [[CrossRef](#)] [[PubMed](#)]
40. Akturk, E.; Akturk, O.U.; Ciraci, S. Single and bilayer bismuthene: Stability at high temperature and mechanical and electronic properties. *Phys. Rev. B* **2016**, *94*, 014115. [[CrossRef](#)]
41. Peng, L.; Xian, J.J.; Tang, P.Z.; Rubio, A.; Zhang, S.C.; Zhang, W.H.; Fu, Y.S. Visualizing topological edge states of single and double bilayer Bi supported on multibilayer Bi(111) films. *Phys. Rev. B* **2018**, *98*, 245108. [[CrossRef](#)]
42. Rasche, B.; Seifert, G.; Enyashin, A. Stability and Electronic Properties of Bismuth Nanotubes. *J. Phys. Chem. C* **2010**, *114*, 22092–22097. [[CrossRef](#)]
43. Zhang, J.D.; Yu, X.F.; Han, W.J.; Lv, B.S.; Li, X.H.; Xiao, S.; Gao, Y.L.; He, J. Broadband spatial self-phase modulation of black phosphorous. *Opt. Lett.* **2016**, *41*, 1704–1707. [[CrossRef](#)] [[PubMed](#)]
44. Zhang, S.L.; Xie, M.Q.; Li, F.Y.; Yan, Z.; Li, Y.F.; Kan, E.J.; Liu, W.; Chen, Z.F.; Zeng, H.B. Semiconducting Group 15 Monolayers: A Broad Range of Band Gaps and High Carrier Mobilities. *Angew. Chem.-Int. Ed.* **2016**, *55*, 1666–1669. [[CrossRef](#)] [[PubMed](#)]
45. Zhou, J.; Chen, J.C.; Chen, M.X.; Wang, J.; Liu, X.Z.; Wei, B.; Wang, Z.C.; Li, J.J.; Gu, L.; Zhang, Q.H.; et al. Few-Layer Bismuthene with Anisotropic Expansion for High-Areal-Capacity Sodium-Ion Batteries. *Adv. Mater.* **2019**, *31*, e1807874. [[CrossRef](#)]
46. Zhang, W.J.; Hu, Y.; Ma, L.B.; Zhu, G.Y.; Zhao, P.Y.; Xue, X.L.; Chen, R.P.; Yang, S.Y.; Ma, J.; Liu, J.; et al. Liquid-phase exfoliated ultrathin Bi nanosheets: Uncovering the origins of enhanced electrocatalytic CO₂ reduction on two-dimensional metal nanostructure. *Nano Energy* **2018**, *53*, 808–816. [[CrossRef](#)]
47. Walker, E.S.; Na, S.R.; Jung, D.; March, S.D.; Kim, J.S.; Trivedi, T.; Li, W.; Tao, L.; Lee, M.L.; Liechti, K.M.; et al. Large-Area Dry Transfer of Single-Crystalline Epitaxial Bismuth Thin Films. *Nano Lett.* **2016**, *16*, 6931–6938. [[CrossRef](#)]
48. Sun, X.H.; Zhao, H.L.; Chen, J.Y.; Zhong, W.; Zhu, B.B.; Tao, L. Effects of the thickness and laser irradiation on the electrical properties of e-beam evaporated 2D bismuth. *Nanoscale* **2021**, *13*, 2648–2657. [[CrossRef](#)] [[PubMed](#)]
49. Shen, J.F.; He, Y.M.; Wu, J.J.; Gao, C.T.; Keyshar, K.; Zhang, X.; Yang, Y.C.; Ye, M.X.; Vajtai, R.; Lou, J.; et al. Liquid Phase Exfoliation of Two-Dimensional Materials by Directly Probing and Matching Surface Tension Components. *Nano Lett.* **2015**, *15*, 5449–5454. [[CrossRef](#)]
50. Huang, Y.X.; Zhu, C.Y.; Zhang, S.L.; Hu, X.M.; Zhang, K.; Zhou, W.H.; Guo, S.Y.; Xu, F.; Zeng, H.B. Ultrathin Bismuth Nanosheets for Stable Na-Ion Batteries: Clarification of Structure and Phase Transition by in Situ Observation. *Nano Lett.* **2019**, *19*, 1118–1123. [[CrossRef](#)]
51. Huo, C.X.; Yan, Z.; Song, X.F.; Zeng, H.B. 2D materials via liquid exfoliation: A review on fabrication and applications. *Sci. Bull.* **2015**, *60*, 1994–2008. [[CrossRef](#)]
52. Li, L.; Zhang, D.; Cao, M.H.; Deng, J.P.; Ji, X.H.; Wang, Q. Electrochemical synthesis of 2D antimony, bismuth and their compounds. *J. Mater. Chem. C* **2020**, *8*, 9464–9475. [[CrossRef](#)]
53. Wu, D.; Shen, X.Q.; Liu, J.W.; Wang, C.; Liang, Y.; Fu, X.Z.; Luo, J.L. Electrochemical exfoliation from an industrial ingot: Ultrathin metallic bismuth nanosheets for excellent CO₂ capture and electrocatalytic conversion. *Nanoscale* **2019**, *11*, 22125–22133. [[CrossRef](#)] [[PubMed](#)]
54. Baboukani, A.R.; Khakpour, I.; Drozd, V.; Wang, C.L. Liquid-Based Exfoliation of Black Phosphorus into Phosphorene and Its Application for Energy Storage Devices. *Small Struct.* **2021**, *2*, 2000148. [[CrossRef](#)]
55. Yang, Z.B.; Hao, J.H. Progress in pulsed laser deposited two-dimensional layered materials for device applications. *J. Mater. Chem. C* **2016**, *4*, 8859–8878. [[CrossRef](#)]
56. Gong, Y.J.; Liu, Z.; Lupini, A.R.; Shi, G.; Lin, J.H.; Najmaei, S.; Lin, Z.; Elias, A.L.; Berkdemir, A.; You, G.; et al. Band Gap Engineering and Layer-by-Layer Mapping of Selenium-Doped Molybdenum Disulfide. *Nano Lett.* **2014**, *14*, 442–449. [[CrossRef](#)]
57. Cai, Z.Y.; Liu, B.L.; Zou, X.L.; Cheng, H.M. Chemical Vapor Deposition Growth and Applications of Two-Dimensional Materials and Their Heterostructures. *Chem. Rev.* **2018**, *118*, 6091–6133. [[CrossRef](#)]
58. Zhu, F.F.; Chen, W.J.; Xu, Y.; Gao, C.L.; Guan, D.D.; Liu, C.H.; Qian, D.; Zhang, S.C.; Jia, J.F. Epitaxial growth of two-dimensional stanene. *Nat. Mater.* **2015**, *14*, 1020–1025. [[CrossRef](#)]
59. Saito, Y.; Nojima, T.; Iwasa, Y. Highly crystalline 2D superconductors. *Nat. Rev. Mater.* **2017**, *2*, 16094. [[CrossRef](#)]
60. Sun, H.-H.; Wang, M.-X.; Zhu, F.; Wang, G.-Y.; Ma, H.-Y.; Xu, Z.-A.; Liao, Q.; Lu, Y.; Gao, C.-L.; Li, Y.-Y.; et al. Coexistence of Topological Edge State and Superconductivity in Bismuth Ultrathin Film. *Nano Lett.* **2017**, *17*, 3035–3039. [[CrossRef](#)]
61. Yaegashi, K.; Sugawara, K.; Kato, T.; Takahashi, T.; Sato, T. Selective Fabrication of Bismuthene and β -Bi on Hydrogen-Terminated SiC(0001). *Langmuir* **2022**, *38*, 13401–13406. [[CrossRef](#)]

62. Nagao, T.; Sadowski, J.T.; Saito, M.; Yaginuma, S.; Fujikawa, Y.; Kogure, T.; Ohno, T.; Hasegawa, Y.; Hasegawa, S.; Sakurai, T. Nanofilm allotrope and phase transformation of ultrathin Bi film on Si(111)-7x7. *Phys. Rev. Lett.* **2004**, *93*, 105501. [[CrossRef](#)] [[PubMed](#)]
63. Jankowski, M.; Kaminski, D.; Vergeer, K.; Mirolo, M.; Carla, F.; Rijnders, G.; Bollmann, T.R.J. Controlling the growth of Bi(110) and Bi(111) films on an insulating substrate. *Nanotechnology* **2017**, *28*, 15. [[CrossRef](#)]
64. Ahmad, H.; Azali, N.A.; Bayang, L.; Yusoff, N. Generation of mode-locked thulium/holmium-doped fiber laser assisted by bismuthene/side polished fiber as saturable absorber. *Laser Phys. Lett.* **2022**, *19*, 7. [[CrossRef](#)]
65. Song, Y.F.; Liang, Z.M.; Jiang, X.T.; Chen, Y.X.; Li, Z.J.; Lu, L.; Ge, Y.Q.; Wang, K.; Zheng, J.L.; Lu, S.B.; et al. Few-layer antimonene decorated microfiber: Ultra-short pulse generation and all-optical thresholding with enhanced long term stability. *2D Mater.* **2017**, *4*, 045010. [[CrossRef](#)]
66. Xu, W.X.; Guo, P.L.; Li, X.H.; Hui, Z.Q.; Wang, Y.M.; Shi, Z.J.; Shu, Y.Q. Sheet-structured bismuthene for near-infrared dual-wavelength harmonic mode-locking. *Nanotechnology* **2020**, *31*, 225209. [[CrossRef](#)] [[PubMed](#)]
67. Chai, T.; Li, X.H.; Feng, T.C.; Guo, P.L.; Song, Y.F.; Chen, Y.X.; Zhang, H. Few-layer bismuthene for ultrashort pulse generation in a dissipative system based on an evanescent field. *Nanoscale* **2018**, *10*, 17617–17622. [[CrossRef](#)]
68. Yang, Q.Q.; Liu, R.T.; Huang, C.; Huang, Y.F.; Gao, L.F.; Sun, B.; Huang, Z.P.; Zhang, L.; Hu, C.X.; Zhang, Z.Q.; et al. 2D bismuthene fabricated via acid-intercalated exfoliation showing strong nonlinear near-infrared responses for mode-locking lasers. *Nanoscale* **2018**, *10*, 21106–21115. [[CrossRef](#)] [[PubMed](#)]
69. Wang, Y.; Ni, W.J.; Set, S.Y.; Yamashita, S.J. Mode-Locked Thulium-Doped Fiber Laser Using a Single-Layer-Graphene-Covered Tapered Fiber. *IEEE Photonics Technol. Lett.* **2017**, *29*, 913–916. [[CrossRef](#)]
70. Du, L.; Lu, D.L.; Li, J.; Yang, K.; Yang, L.L.; Huang, B.; Yi, J.; Yi, Q.; Miao, L.L.; Qi, X.; et al. Broadband Nonlinear Optical Response of Single-Crystalline Bismuth Thin Film. *ACS Appl. Mater. Interfaces* **2019**, *11*, 35863–35870. [[CrossRef](#)]
71. Chen, H.L.; Zhou, M.; Zhang, P.X.; Yin, H.; Zhu, S.Q.; Li, Z.; Chen, Z.Q. Passively Q-switched Nd:GYAP laser at 1.3 μm with bismuthene nanosheets as a saturable absorber. *Infrared Phys. Technol.* **2022**, *121*, 104023. [[CrossRef](#)]
72. Dong, L.; Li, D.C.; Pan, H.; Li, Y.; Zhao, S.Z.; Li, G.Q.; Chu, H.W. Pulse characteristics from a MoSe₂ Q-switched Nd:GdVO₄ laser at 1.3 μm . *Appl. Opt.* **2019**, *58*, 8194–8199. [[CrossRef](#)]
73. Lin, M.X.; Peng, Q.Q.; Hou, W.; Fan, X.W.; Liu, J. 1.3 μm Q-switched solid-state laser based on few-layer ReS₂ saturable absorber. *Opt. Laser Technol.* **2019**, *109*, 90–93. [[CrossRef](#)]
74. Feng, X.Y.; Hao, Q.Q.; Lin, Y.K.; Yu, X.R.; Wu, Q.H.; Huang, H.; Zhang, F.; Liu, J.; Su, L.B.; Zhang, H. Bismuth nanosheets Q-switched Nd:BGO laser operating at 1065 nm with 880 nm laser-diode pumping. *Opt. Laser Technol.* **2020**, *127*, 106152. [[CrossRef](#)]
75. Du, J.; Wang, Q.K.; Jiang, G.B.; Xu, C.W.; Zhao, C.J.; Xiang, Y.J.; Chen, Y.; Wen, S.C.; Zhang, H. Ytterbium-doped fiber laser passively mode locked by few-layer Molybdenum Disulfide (MoS₂) saturable absorber functioned with evanescent field interaction. *Sci. Rep.* **2014**, *4*, 6346. [[CrossRef](#)] [[PubMed](#)]
76. Wang, J.T.; Jiang, Z.K.; Chen, H.; Li, J.R.; Yin, J.D.; Wang, J.Z.; He, T.C.; Yan, P.G.; Ruan, S.C. High energy soliton pulse generation by a magnetron-sputtering-deposition-grown MoTe₂ saturable absorber. *Photonics Res.* **2018**, *6*, 535–541. [[CrossRef](#)]
77. Liu, W.J.; Pang, L.H.; Han, H.N.; Bi, K.; Lei, M.; Wei, Z.Y. Tungsten disulphide for ultrashort pulse generation in all-fiber lasers. *Nanoscale* **2017**, *9*, 5806–5811. [[CrossRef](#)] [[PubMed](#)]
78. Niu, K.D.; Sun, R.Y.; Chen, Q.Y.; Man, B.Y.; Zhang, H.N. Passively mode-locked Er-doped fiber laser based on SnS₂ nanosheets as a saturable absorber. *Photonics Res.* **2018**, *6*, 72–76. [[CrossRef](#)]
79. Xu, Y.H.; Xie, H.H.; Jiang, G.B.; Miao, L.L.; Wang, K.; Tang, S.Y.; Yu, X.F.; Zhang, H.; Bao, Q.L. Bilayer Bismuth Selenide nanoplatelets based saturable absorber for ultra-short pulse generation (Invited). *Opt. Commun.* **2017**, *395*, 55–60. [[CrossRef](#)]
80. Tian, X.L.; Wei, R.F.; Liu, M.; Zhu, C.H.; Luo, Z.C.; Wang, F.Q.; Qiu, J.R. Ultrafast saturable absorption in TiS₂ induced by non-equilibrium electrons and the generation of a femtosecond mode-locked laser. *Nanoscale* **2018**, *10*, 9608–9615. [[CrossRef](#)] [[PubMed](#)]
81. Huang, W.C.; Zhu, J.; Wang, M.K.; Hu, L.P.; Tang, Y.F.; Shu, Y.Q.; Xie, Z.J.; Zhang, H. Emerging Mono-Elemental Bismuth Nanostructures: Controlled Synthesis and Their Versatile Applications. *Adv. Funct. Mater.* **2021**, *31*, 2007584. [[CrossRef](#)]
82. Babu, S.S.; Muthuraja, P.; Yadav, P.; Gopinath, P. Aryldiazonium Salts in Photoredox Catalysis—Recent Trends. *Adv. Synth. Catal.* **2021**, *363*, 1782–1809. [[CrossRef](#)]
83. Mo, F.Y.; Qiu, D.; Zhang, L.; Wang, J.B. Recent Development of Aryl Diazonium Chemistry for the Derivatization of Aromatic Compounds. *Chem. Rev.* **2021**, *121*, 5741–5829. [[CrossRef](#)] [[PubMed](#)]
84. Wang, Z.; Li, C.; Domen, K. Recent developments in heterogeneous photocatalysts for solar-driven overall water splitting. *Chem. Soc. Rev.* **2019**, *48*, 2109–2125. [[CrossRef](#)] [[PubMed](#)]
85. Li, Y.Y.; Fan, J.S.; Tan, R.Q.; Yao, H.C.; Peng, Y.; Liu, Q.C.; Li, Z.J. Selective Photocatalytic Reduction of CO₂ to CH₄ Modulated by Chloride Modification on Bi₂WO₆ Nanosheets. *ACS Appl. Mater. Interfaces* **2020**, *12*, 54507–54516. [[CrossRef](#)]
86. Chen, Y.; Wang, F.; Cao, Y.H.; Zhang, F.Y.; Zou, Y.Z.; Huang, Z.A.; Ye, L.Q.; Zhou, Y. Interfacial Oxygen Vacancy Engineered Two-Dimensional g-C₃N₄/BiOCl Heterostructures with Boosted Photocatalytic Conversion of CO₂. *ACS Appl. Energy Mater.* **2020**, *3*, 4610–4618. [[CrossRef](#)]

87. Ma, Z.Y.; Li, P.H.; Ye, L.Q.; Zhou, Y.; Su, F.Y.; Ding, C.H.; Xie, H.Q.; Bai, Y.; Wong, P.K. Oxygen vacancies induced exciton dissociation of flexible BiOCl nanosheets for effective photocatalytic CO₂ conversion. *J. Mater. Chem. A* **2017**, *5*, 24995–25004. [[CrossRef](#)]
88. Ge, M.; Yang, C.L.; Wang, M.S.; Ma, X.G. Photocatalytic hydrogen generation from overall water splitting with direct Z-scheme driven by two-dimensional InTe/Bismuthene heterostructure. *Int. J. Hydrog. Energy* **2023**, *48*, 138–146. [[CrossRef](#)]
89. Xie, Z.J.; Xing, C.Y.; Huang, W.C.; Fan, T.J.; Li, Z.J.; Zhao, J.L.; Xiang, Y.J.; Guo, Z.N.; Li, J.Q.; Yang, Z.G.; et al. Ultrathin 2D Nonlayered Tellurium Nanosheets: Facile Liquid-Phase Exfoliation, Characterization, and Photoresponse with High Performance and Enhanced Stability. *Adv. Funct. Mater.* **2018**, *28*, 1705833. [[CrossRef](#)]
90. Xing, C.Y.; Huang, W.C.; Xie, Z.J.; Zhao, J.L.; Ma, D.T.; Fan, T.J.; Liang, W.Y.; Ge, Y.Q.; Dong, B.Q.; Li, J.Q.; et al. Ultrasmall Bismuth Quantum Dots: Facile Liquid-Phase Exfoliation, Characterization, and Application in High-Performance UV-Vis Photodetector. *ACS Photonics* **2018**, *5*, 621–629. [[CrossRef](#)]
91. Wang, B.; Zhou, Y.; Huang, Z.; Qiao, H.; Duan, C.; Ren, X.; Wang, Z.; Zhong, J.; Qi, X. Photoelectrochemical self-powered photodetector based on 2D liquid-exfoliated bismuth nanosheets: With novel structures for portability and flexibility. *Mater. Today Nano* **2021**, *14*, 100109. [[CrossRef](#)]
92. Ren, X.H.; Li, Z.J.; Huang, Z.Y.; Sang, D.; Qiao, H.; Qi, X.; Li, J.Q.; Zhong, J.X.; Zhang, H. Environmentally Robust Black Phosphorus Nanosheets in Solution: Application for Self-Powered Photodetector. *Adv. Funct. Mater.* **2017**, *27*, 1606834. [[CrossRef](#)]
93. Yao, J.D.; Zheng, Z.Q.; Shao, J.M.; Yang, G.W. Promoting Photosensitivity and Detectivity of the Bi/Si Heterojunction Photodetector by Inserting a WS₂ Layer. *ACS Appl. Mater. Interfaces* **2015**, *7*, 26701–26708. [[CrossRef](#)] [[PubMed](#)]
94. Pataniya, P.M.; Sumesh, C.K. WS₂ Nanosheet/Graphene Heterostructures for Paper-Based Flexible Photodetectors. *ACS Appl. Nano Mater.* **2020**, *3*, 6935–6944. [[CrossRef](#)]
95. Pataniya, P.; Solanki, G.K.; Patel, K.D.; Pathak, V.M.; Sumesh, C.K. Crystal growth, characterization and photo detection properties of 2H-V_{0.75}W_{0.25}Se₂ ternary alloy with 1T-VSe₂ secondary phase. *Mater. Res. Express* **2017**, *4*, 106306. [[CrossRef](#)]
96. Chauhan, B.L.; Bhakhar, S.A.; Pataniya, P.M.; Gupta, S.U.; Solanki, G.K.; Pathak, V.M.; Patel, V. Liquid-phase exfoliation of WSe₂ nanosheets for ITO/WSe₂ photodetector. *J. Mater. Sci.-Mater. Electron.* **2022**, *33*, 10314–10322. [[CrossRef](#)]

Disclaimer/Publisher's Note: The statements, opinions and data contained in all publications are solely those of the individual author(s) and contributor(s) and not of MDPI and/or the editor(s). MDPI and/or the editor(s) disclaim responsibility for any injury to people or property resulting from any ideas, methods, instructions or products referred to in the content.